

Geo-spatial Information Science



ISSN: 1009-5020 (Print) 1993-5153 (Online) Journal homepage: www.tandfonline.com/journals/tgsi20

Improving multipath extraction in PPP-RTK for high-precision dynamic deformation monitoring

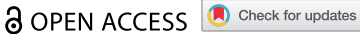
Xinrui Li, Bao Shu, Xuanyu Qu, Qin Zhang, Yunqing Tian, Guanwen Huang & Li Wang

To cite this article: Xinrui Li, Bao Shu, Xuanyu Qu, Qin Zhang, Yunqing Tian, Guanwen Huang & Li Wang (20 Aug 2025): Improving multipath extraction in PPP-RTK for high-precision dynamic deformation monitoring, Geo-spatial Information Science, DOI: 10.1080/10095020.2025.2543971

To link to this article: https://doi.org/10.1080/10095020.2025.2543971

| <u>a</u> | © 2025 Wuhan University. Published by Informa UK Limited, trading as Taylor & Francis Group. |
|-----------|--|
| | Published online: 20 Aug 2025. |
| | Submit your article to this journal 🗗 |
| hh | Article views: 423 |
| α | View related articles 🗹 |
| CrossMark | View Crossmark data 🗗 |







Improving multipath extraction in PPP-RTK for high-precision dynamic deformation monitoring

Xinrui Li^{a,b}, Bao Shu^{a,b}, Xuanyu Qu^oc, Qin Zhang^{a,b}, Yunqing Tian^{a,b}, Guanwen Huang^{a,b} and Li Wang^{a,b}

^aCollege of Geological Engineering and Geomatics, Chang'an University, Xi'an, China; ^bKey Laboratory of Western China's Mineral Resources and Geological Engineering, Ministry of Education, Xi'an, China; Department of Land Surveying and Geo-Informatics, The Hong Kong Polytechnic University, Hong Kong, China

ABSTRACT

Multipath error is one of the most critical error sources in GNSS precise-positioning applications. Extracting accurate observational residuals is a fundamental and challenging task for constructing multipath corrections in a Precision Point Positioning Real-Time Kinematics (PPP-RTK) model. We proposed a novel multipath extraction method in UnDifferenced and UnCombined (UDUC) PPP-RTK framework. Instead of extracting multipath directly from UD residuals, our method first extracts inter-satellite Single-Difference (SD) residuals and then converts them to UD residuals. Additionally, we replace the fixed average position parameters used in traditional multipath modeling with trends that reflect the true deformation at the station, accommodating both stable and dynamic motion scenarios. Experimental results in real landslide scenarios demonstrate that the proposed method reduces the impact of receiver clock offset and other satellite ambiguity parameters on residual extraction and is suitable for both stable and dynamic motion conditions. Results from two reference networks with average spacings of 105 km and 214 km demonstrate that the proposed method achieved positioning accuracies of 1.1 cm, 1.2 cm, 3.2 cm in the east, north, up directions, and 1.0 cm, 1.3 cm, 3.3 cm, respectively. Compared to the traditional multipath extraction method that uses averaged position parameters, these results represent improvements of 15%, 14%, 20%, and 37%, 28%, 23%, respectively.

ARTICLE HISTORY

Received 24 October 2024 Accepted 31 July 2025

KEYWORDS

PPP-RTK; multipath mitigation; undifferenced residuals; landslide; deformation monitoring

1. Introduction

The application of the Global Navigation Satellite System (GNSS) in deformation monitoring is widespread, such as deformation monitoring (Bock 1991), bridges (Qu et al. 2023), and buildings (Lovse et al. 1995), due to the capabilities of GNSS in obtain realtime three-dimensional displacements under diverse weather conditions. Currently, deformation monitoring based on GNSS primarily utilizes Real-Time Kinematic (RTK) technology. Although this method can achieve high-precision results, its deployment model suffers from high costs, low utilization of reference stations, and an over-reliance on a single reference station, which limits its widespread application. While the Precise Point Positioning (PPP) and Network RTK (NRTK) technologies can overcome these issues, PPP struggles with positioning accuracy and convergence time (Kazmierski, Zajdel, and Sośnica 2020), and NRTK is sensitive to atmospheric modeling errors and has a heavy data communication burden (Cina et al. 2015).

To fully leverage the advantages of PPP and RTK technologies and overcome their limitations, PPP-RTK technology has been developed through the

application of Ambiguity Resolution (AR) and atmospheric corrections to the PPP model (Teunissen, Odijk, and Zhang 2010; Wübbena, Schmitz, and Bagge 2005). This technology enables rapid AR with a single receiver by utilizing precise correction products derived from ground reference networks, such as accurate satellite orbits and clock offset, ionospheric, and tropospheric delays (Li, Zhang, and Ge 2011), and Uncalibrated Phase Delay (UPD, Ge et al. 2008).

Multipath remains one of the major challenges in high-precision PPP-RTK positioning applications. The mainstream methods for mitigating multipath are generally based on the use of the spatiotemporal repetitiveness of satellite orbits, including Sidereal Filtering (SF, Bock 1991; Elosegui et al. 1995) and Multipath Hemispherical Map (MHM, Dong et al. 2016). The former is based on the temporal repetitiveness of satellites, while the latter (MHM) only relies on the satellites' location repeatability in space. Bock (1991) first introduced the concept of SF in 1991 and applied it for coordinate domain multipath mitigation. Ragheb, Clarke, and Edwards (2007) applied SF to the Double-Differences (DD)

observation domain. Zhong et al. (2010) converted DD residuals to inter-station Single-Differences (SD), establishing individual satellite multipath correction models, which proved superior to the DD method. Geng, Jiang, and Liu (2017) analyzed the applicability of the SF model under PPP and successfully mitigated multipath effects in both coordinate and carrier-phase residuals. The implementation of the SF involves the denoising process on coordinate sequences or observation residuals using digital filtering technologies, including low-pass filtering (Zhong et al. 2010), wavelet (Azarbad and Mosavi 2014), Singular Spectrum Analysis Multichannel-SSA (MSSA, Li et al. 2024), and their variants (Dai, Huang, and Cai 2014).

In contrast, the value of multipath correction in the MHM method, which is based on the spatial domain, is solely dependent on the satellite's position and remains independent of individual satellite characteristics (Cohen and Parkinson 1991). Dong et al. (2016) compared MHM with SF/advanced SF methods and demonstrated that MHM may encounter difficulties when mitigating high-frequency multipath. Wang et al. (2019) developed a trend surface analysis-based MHM (TMHM) method for handling this. Zheng et al. (2019) and Lu et al. (2021) applied MHM and TMHM to the PPP model and analyzed their performance, demonstrating that TMHM further improves positioning accuracy and reduces convergence time compared to the MHM model. Gao et al. (2023) generated a multipath correction model based on UD residuals in the PPP-RTK framework and successfully applied it for multipath mitigation at a bridge monitoring station.

Extracting accurate observation residuals from historical data is crucial for establishing a high-precision multipath correction model and achieving effective multipath mitigation (Chen et al. 2022). During the PPP AR process (Shu et al. 2024), incorrect ambiguity fixes for certain satellites are inevitable due to the varying difficulty in resolving ambiguities for different satellites (Ge et al. 2008; Ogutcu et al. 2023). These errors affect the accuracy of UD residual extraction for all satellites as the estimation process progresses. Furthermore, since position parameters and multipath errors are inseparable (Kaloop et al. 2020; Wang et al. 2023), the position parameters are precomputed and fixed by averaging results over multiple days during the multipath error extraction process (Atkins and Ziebart 2016; Choi et al. 2004; Geng et al. 2018). This approach is reasonable for static stations. However, for deformation monitoring stations, such as those on bridges or in landslide-prone areas, where continuous deformation occurs, using average position parameters introduces position errors into the observation residuals.

To address these deficiencies, we optimized the multipath extraction method in the PPP-RTK

technique, aiming to improve the accuracy and robustness of the constructed multipath correction model. This development is based on recovering accurate UD residuals from inter-satellite SD residuals, effectively eliminating the influence of receiver clock offsets and ambiguity parameters between satellites on residual extraction. Furthermore, we proposed an effective and easy-to-implement multipath extraction method specifically designed for dynamic monitoring scenarios. We evaluated the performance of our method in PPP-RTK deformation monitoring using datasets collected from a realworld landslide site, which included both stable and moving monitoring points. The methods used to assess the accuracy of multipath extraction included SF, MHM, and TMHM. During the experiment, we successfully recorded the entire process a landslide collapse event.

2. Methodology

This section begins by detailing the GNSS observation equations for the UnDifferenced and UnCombined (UDUC) model. Then, the AR method of UDUC PPP-RTK is described. Subsequently, the section outlines two distinct methods for extracting UD residuals and a multipath extraction technique suitable for dynamic monitoring stations.

2.1. GNSS observation equations of the UDUC model

The linearized equations for GNSS code and phase observables are given below (Li et al. 2014; Odijk et al. 2016):

$$P_{r,i}^{s} = \rho_{r}^{s} + c \cdot dt_{r} - c \cdot dt^{s} + m \cdot T_{r} + \gamma_{i} \cdot I_{r,1}^{s} + b_{r,i}$$

$$- b_{i}^{s} + (MP_{Pi} + \varepsilon_{Pi})$$

$$L_{r,i}^{s} = \rho_{r}^{s} + c \cdot dt_{r} - c \cdot dt^{s} + m \cdot T_{r} - \gamma_{i} \cdot I_{r,1}^{s} + \lambda_{i}$$

$$\cdot N_{r,i}^{s} + \lambda_{i} \cdot (B_{r,i} - B_{i}^{s}) + (MP_{Li} + \varepsilon_{Li})$$

$$(1)$$

where P and L represent pseudorange and carrier-phase observation values, respectively; s and r are satellite and station indexes, respectively; i represents the carrier frequency (i=1,2); ρ is the geometric distance form the satellite antenna-phase center to the receiver-phase center; c is the speed of light in vacuum; dt_r and dt^s are the receiver clock offset and satellite clock offset, respectively; T_r and m are the tropospheric zenith wet delay and the corresponding mapping function, respectively; $\gamma_i = \frac{f_i^2}{f_i^2}$ is the ionospheric coefficient on frequency i; f is the frequency value; $f_{r,1}^s$ is the slant ionospheric delay from the receiver to the satellite on frequency 1; λ_i is the wavelength; $N_{r,i}^s$ is the integer-phase

Table 1. Estimatable parameters of the reparameterized UDUC PPP equation for PPP-RTK.

| Estimable Parameter | Formulation | | | | | | |
|---|---|--|--|--|--|--|--|
| $\bar{d}t_r$ | $dt_r + d_{IF,r}/c$ | | | | | | |
| dt _r dt⁵ | $dt^{s}+d_{IF}^{s}/c$ | | | | | | |
| $\overline{I}_{r,1}^{s}$ | $I_{r,1}^s + \beta \cdot (DCB_r - DCB^s)$ | | | | | | |
| $egin{array}{l} ar{I}_{r,1}^s \ ar{N}_{r,i}^s \ ar{arepsilon}_{ar{arepsilon}_{ar{l}i}} \end{array}$ | $N_{r,i}^{s} + B_{r,i} - B_{i}^{s} - \left[d_{IF,r} - d_{IF}^{s} - \gamma_{i} \cdot \beta \cdot (DCB_{r} - DCB^{s})\right]/\lambda_{i}$ | | | | | | |
| $\overline{\varepsilon}_{Pi}$ | $M_{Pi} + arepsilon_{Pi}$ | | | | | | |
| ĒLi | $M_{Li} + \epsilon_{Li}$ | | | | | | |

Note: $d_{IF,r} = a \cdot b_{r,1} + \beta \cdot b_{r,2}$; $d_{IF}^s = a \cdot b_1^s + \beta \cdot b_2^s$; $a = \frac{f_1^2}{f_1^2 - f_2^2}$, $\beta = -\frac{f_2^2}{f_1^2 - f_2^2}$, $DCB_r = b_{r,1} - b_{r,2}$, $DCB^s = b_1^s - b_2^s$.

ambiguity; $b_{r,i}$ ($B_{r,i}$) and b_i^s (B_i^s) are the pseudorange (phase) hardware delays of the receiver and satellite, respectively; MP_{Pi} (ε_{Pi}) and MP_{Li} (ε_{Li}) denote the multipath errors (observation noise) for pseudorange and phase, respectively.

In UDUC PPP data processing, the satellite clock offset uses the ionospheric-free combined clock offset product of the IGS. The precise clock offset includes the satellite pseudorange hardware delay deviation, which requires hardware delay correction. At the same time, reparameterization parameters often need to be estimated due to correlations between receiver clock offsets, satellite clock offsets, ionospheric delays, and hardware delay parameters for carrier phase and pseudorange. Furthermore, since the multipath and observation noise are difficult to be separated, multipath is usually incorporated into the observation noise. Therefore, the reparameterized estimated parameters of this model are defined as follows (Table 1, Teunissen, Odijk, and Zhang 2010; Zhang, Chen, and Yuan 2019):

$$P_{r,i}^{s} = \rho_{r}^{s} + c \cdot \overline{d}t_{r} - c \cdot \overline{d}t^{s} + m \cdot T_{r} + \gamma_{i} \cdot \overline{I}_{r,1}^{s} + \overline{\epsilon}_{Pi}L_{r,i}^{s}$$

$$= \rho_{r}^{s} + c \cdot \overline{d}t_{r} - c \cdot \overline{d}t^{s} + m \cdot T_{r} - \gamma_{i} \cdot \overline{I}_{r,1}^{s} + \lambda_{i}$$

$$\cdot \overline{N}_{r,i}^{s} + \overline{\epsilon}_{Li}$$
(2)

where $\bar{d}t_r$ and $\bar{d}t^s$ is the receiver clock offset and satellite clock offset after reparameterization, respectively; $\bar{I}_{r,1}^s$, $\bar{N}_{r,i}^s$, and $\bar{\varepsilon}_{Li}$ are the slant ionospheric delay, phase ambiguity, and observation noise after reparameterization, respectively. DCB_r and DCB^s are the differenced code hardware delays between frequencies 1 and 2 for receiver and satellite, respectively.

2.2. Ambiguity resolution in UDUC PPP-RTK

Correct ambiguity resolution is crucial for enhancing positioning accuracy and reducing the convergence time at the user end. This paper employs Observable-Specific code Bias (OSB) products for phase bias correction at the satellite end, directly obtaining integer characteristics of SD inter-satellite ambiguities. The phase observation equations are adjusted to directly

estimate the Wide-Lane (WL) and Narrow-Lane (NL) ambiguities (Liu et al. 2020; Shu et al. 2024). For instance, using dual-frequency phase observations:

$$L_{r,1}^{s} + b_{L1}^{s} = \rho_{r}^{s} + c \cdot \bar{d}t_{r} - c \cdot \bar{d}t^{s} + m \cdot T_{r} - \gamma_{1} \cdot \bar{I}_{r,1}^{s} + \lambda_{1} \cdot \bar{N}_{r,1}^{s} + \bar{\epsilon}_{L1} L_{r,2}^{s} + b_{L2}^{s}$$

$$= \rho_{r}^{s} + c \cdot \bar{d}t_{r} - c \cdot \bar{d}t^{s} + m \cdot T_{r} - \gamma_{2} \cdot \bar{I}_{r,1}^{s} + \lambda_{2} \cdot \left(\bar{N}_{r,1}^{s} - \bar{N}_{r,WL}^{s}\right) + \bar{\epsilon}_{L2}$$

$$(3)$$

where $\bar{N}_{r,1}^s = \bar{N}_{r,NL}^s$. b_{Li}^s are carrier-phase OSB, which can be directly obtained by Centre National d' Etudes Spatiales (CNES) analysis center. The specific process is as follows:

I. Based on the Kalman filter method, the UDUC PPP float solution is obtained, which eliminates the influence of satellite-end UPD on the float WL and NL ambiguities.

$$V = \mathbf{B}\bar{X} - L, \mathbf{P} \tag{4}$$

$$\bar{X} = (\mathbf{B}^{\mathrm{T}}\mathbf{P}\mathbf{B})^{-1}(\mathbf{B}^{\mathrm{T}}\mathbf{P}L) = \mathbf{H}^{-1}W$$
 (5)

where, Equation (4) represents the error equation of the UDUC PPP float solution, with Equation (5) are the float solution itself. H and W are the normal equations and constants of the float solution, respectively.

II. To avoid the impact of UPD at the receiver-end, SD inter-satellite processing is performed on the WL ambiguity parameters. The WL ambiguity-fixed solution is then obtained using the rounding method and is imposed as a pseudo-observation constraint into the normal equation and constants of the UDUC PPP float solution. The error equation constrained by the SD inter-satellite WL integer ambiguity is transformed as follows:

$$V_{\Delta N_{WI}} = B_{\Delta N_{WI}} \bar{X}_1 - L_{\Delta N_{WI}}, P_{\Delta N_{WI}}$$
 (6)

The original float solution changes to:

$$\bar{X}_1 = \boldsymbol{H}_1^{-1} W_1
\boldsymbol{H}_1 = \boldsymbol{H} + \boldsymbol{B}_{\Delta N_{WL}}^T \boldsymbol{P}_{\Delta N_{WL}} \boldsymbol{B}_{\Delta N_{WL}}
W_1 = W + \boldsymbol{B}_{\Delta N_{WL}}^T \boldsymbol{P}_{\Delta N_{WL}} L_{\Delta N_{WL}}$$
(7)

III. The NL ambiguities in the new float solution X_1 are processed through SD inter-satellite, followed by a LAMBDA (Least-square AMBiguity Decorrelation Adjustment) search to obtain the SD inter-satellite NL ambiguity-fixed solution. Let s_0 represent the reference satellite; then, the SD inter-satellite and LAMBDA-derived NL ambiguities can be, respectively, represented as follows:

$$\Delta \bar{N}_{r,NL}^{s,s_0} = \bar{N}_{r,NL}^s - \bar{N}_{r,NL}^{s_0} \tag{8}$$

$$\Delta \hat{N}_{r,NL}^{s,s_0} = LAMBDA(\Delta \bar{N}_{r,NL}^{s,s_0})$$
 (9)

IV. These SD inter-satellite NL ambiguity-fixed solutions are then imposed as pseudo-observation constraints into the ambiguity normal equation and constants, allowing for the resolution of the constrained updated UDUC ambiguity parameters and other estimable parameters.

$$V_{\Delta N_{\rm NL}} = \mathbf{B}_{\Delta N_{\rm NL}} \hat{X} - L_{\Delta N_{\rm NL}}, \mathbf{P}_{\Delta N_{\rm NL}}$$
 (10)

$$\hat{X} = \mathbf{H}_2^{-1} W_2 \tag{11}$$

$$H_2 = H_1 + \boldsymbol{B}_{\Delta N_{NL}}^T \boldsymbol{P}_{\Delta N_{NL}} \boldsymbol{B}_{\Delta N_{NL}}$$

$$W_2 = W_1 + \boldsymbol{B}_{\Delta N_{NL}}^T \boldsymbol{P}_{\Delta N_{NL}} \boldsymbol{L}_{\Delta N_{NL}}$$
(12)

2.3. UDUC PPP-RTK multipath extraction

Since position parameters are difficult to separate from multipath errors, it is necessary to fix position parameters in advance during multipath extraction, rather than including them in the estimation. In static environments, the station location information can be determined by averaging the positioning results over several days. In this context, the external correction information under the PPP-RTK model includes the receiver's position, satellite orbits and clock offsets, OSB, tropospheric delay and ionospheric delays. The ionospheric and tropospheric correction values are introduced into the observation equation as pseudo-observations, assigning observational weights to constrain these parameters (Gao et al. 2023). $\hat{X} = \left[\hat{d}t_r, \hat{T}_r, \hat{I}^s_{r,1}, \hat{N}^s_{r,NL}, \hat{N}^s_{r,WL}\right]$. Therefore, the residuals under the UDUC PPP model can be calculated as follows:

$$\hat{\varepsilon}_{Li} = L_{r,i}^s + \tilde{b}_{Li}^s - \tilde{\rho}_r^s - c \cdot \hat{d}t_r + c \cdot \tilde{d}t^s - m \cdot \hat{T}_r + \gamma_i \cdot \hat{I}_{r,1}^s - \lambda_i \cdot \hat{N}_{r,i}^s$$
(13)

where "~" represents external correction data; when i=2, it can be calculated first $\hat{N}_{r,2}^s=\hat{N}_{r,1}^s-\hat{N}_{r,WL}^s$, then put it into Equation (13) to calculate the residual of frequency 2.

In addition to Equation (13), residuals can also be calculated using the SD inter-satellite integer

ambiguity $\Delta \hat{N}_{r,NL}^{s,s_0}$ plus the float ambiguity $\hat{N}_{r,NL}^{s_0}$ of the reference satellite:

$$\hat{\varepsilon}_{Li} = L_{r,i}^{s} + \tilde{b}_{Li}^{s} - \tilde{\rho}_{r}^{s} - c \cdot \hat{d}t_{r} + c \cdot \tilde{d}t^{s} - m \cdot \hat{T}_{r} + \gamma_{i}$$

$$\cdot \hat{I}_{r,1}^{s} - \lambda_{i} \cdot \left(\Delta \hat{N}_{r,i}^{s,s_{0}} + \hat{N}_{r,i}^{s_{0}}\right)$$
(14)

It can be observed that the two methods differ only in the way of ambiguity calculation. As shown, the values of $\hat{N}_{r,i}^s$ and $\hat{N}_{r,i}^{s_0}$ are obtained by updating the constraint from $\Delta \hat{N}_{r,i}^{s,s_0}$, which means that the UD residuals calculated by both methods are equivalent.

Due to the varying difficulty of ambiguities-fixing for each satellite, if an incorrect fix occurs for a satellite's NL ambiguity after SD inter-satellite, it will affect all the constrained updated parameters (Liu, Zhang, and Li 2019). However, according to Equation (8) and (9), $\Delta \hat{N}_{r,i}^{s,s_0}$ is not influenced by incorrect ambiguity fixes from other satellites. Therefore, this paper proposes a novel residual extraction method that directly uses SD ambiguity parameters to convert SD residuals to UD residuals. The first step is to obtain the inter-satellite SD residuals:

$$\Delta \hat{\varepsilon}_{Li}^{s,s_0} = \hat{\varepsilon}_{Li}^{s} - \hat{\varepsilon}_{Li}^{s_0} \\
= \Delta L_{r,i}^{s,s_0} + \Delta \tilde{b}_{Li}^{s,s_0} - \Delta \tilde{\rho}_{r}^{s,s_0} + c \cdot \Delta \tilde{d} t^{s,s_0} - m \\
\cdot \Delta \hat{T}_{r,i}^{s,s_0} + \gamma_i \cdot \Delta \hat{I}_{r,1}^{s,s_0} - \lambda_i \cdot \Delta \hat{N}_{r,i}^{s,s_0} \tag{15}$$

The relationship between SD and UD residuals can be expressed as:

$$\mathbf{D}u = s \tag{16}$$

where D is a coefficient matrix; u is the vector of UD residuals and s is the vector of SD residuals. It can be observed that **D** is singular and cannot be inverted. Referring to the method of converting DD residuals to SD residuals in the RTK model (Zhong et al. 2010), and considering that recovering UD residuals from SD residuals is not sensitive to different weighting strategies (Zhong et al. 2010), by adding zero-mean constraints $\sum_{r=1}^{n} w_s u_r^s = 0, \text{ where } w_s = \sin^2(\theta) \text{ makes } \boldsymbol{D} \text{ invertible.}$ Thus, UD residuals can be solved by inverting *D*:

$$\begin{bmatrix} w_1 & w_2 & w_3 & \dots & w_n \\ -1 & 1 & 0 & \dots & 0 \\ -1 & 0 & 1 & \dots & 0 \\ & & \dots & & \\ -1 & 0 & 0 & \dots & 1 \end{bmatrix} \begin{bmatrix} u_r^1 \\ u_r^2 \\ u_r^3 \\ \dots \\ u_r^n \end{bmatrix}$$

$$= \begin{bmatrix} \sum w_s u_r^s = 0 \\ s_r^{12} \\ s_r^{13} \\ \dots \\ s_r^{1n} \end{bmatrix}$$
(17)

where w_s and θ represent the weight and elevation angle corresponding to satellite s, respectively. Although the introduction of zero-mean constraints in the coefficient matrix **D** during the conversion of SD residuals to UD residuals may cause some error propagation when one satellite's ambiguity is incorrectly fixed, the magnitude of this error is significantly smaller compared to the impact of incorrect ambiguity parameters. Furthermore, the influence of incorrect ambiguity fixes on the accuracy of residual extraction for other satellites will be discussed in detail in the subsequent sections.

For ease of description, we refer to the conventional residual extraction method based on Equation (13) or Equation (14) as UD residuals. The proposed method that converts SD to UD residuals (Equations (15), (16)) is abbreviated as SDtoUD hereafter. From Equation (15), it can be seen that SDtoUD residuals eliminate the influence of receiver clock offset and UD ambiguity parameters, leaving only atmospheric parameters in the estimated values affected by incorrect ambiguity fixes from other satellites.

2.4. Multipath extraction for continuously deforming stations

Most previous studies considered the monitoring point to be stable when extracting multipath errors and constructing a multipath correction model. Due to the high satellite orbit height, when the station undergoes centimeter-level deformation (assuming that the attenuation coefficient remains unchanged), the effect on the carrier-

phase observation error can be neglected (Elosegui et al. 1995). In this case, multipath errors still exhibit periodic repeatability related to the station environment (Dai, Ding, and Zhu 2008; Guo et al. 2024; Li et al. 2024). Therefore, existing multipath mitigation methods (such as SF, MHM, etc.) can still be effectively utilized if the multipath errors in dynamic deformation scenarios can be accurately extracted.

For stations in dynamic deformation scenarios, displacement may occur at every epoch. The key to extracting multipath errors in such scenarios is accurately determining the antenna position. Based on this, this paper proposes a dynamic position parameter-based multipath extraction method. By extracting trend components from the original coordinate time series and using these trends as the actual position parameters, accurate multipath values can be extracted, and a multipath correction model can be established. Figure 1 illustrates the flowchart of the PPP-RTK multipath mitigation algorithm suitable for dynamic deformation monitoring, utilizing the SDtoUD multipath extraction method. The process can be divided into four steps:

(I) The coordinate time series of the period corresponding to the multipath modeling data is solved to determine whether deformation occurs.

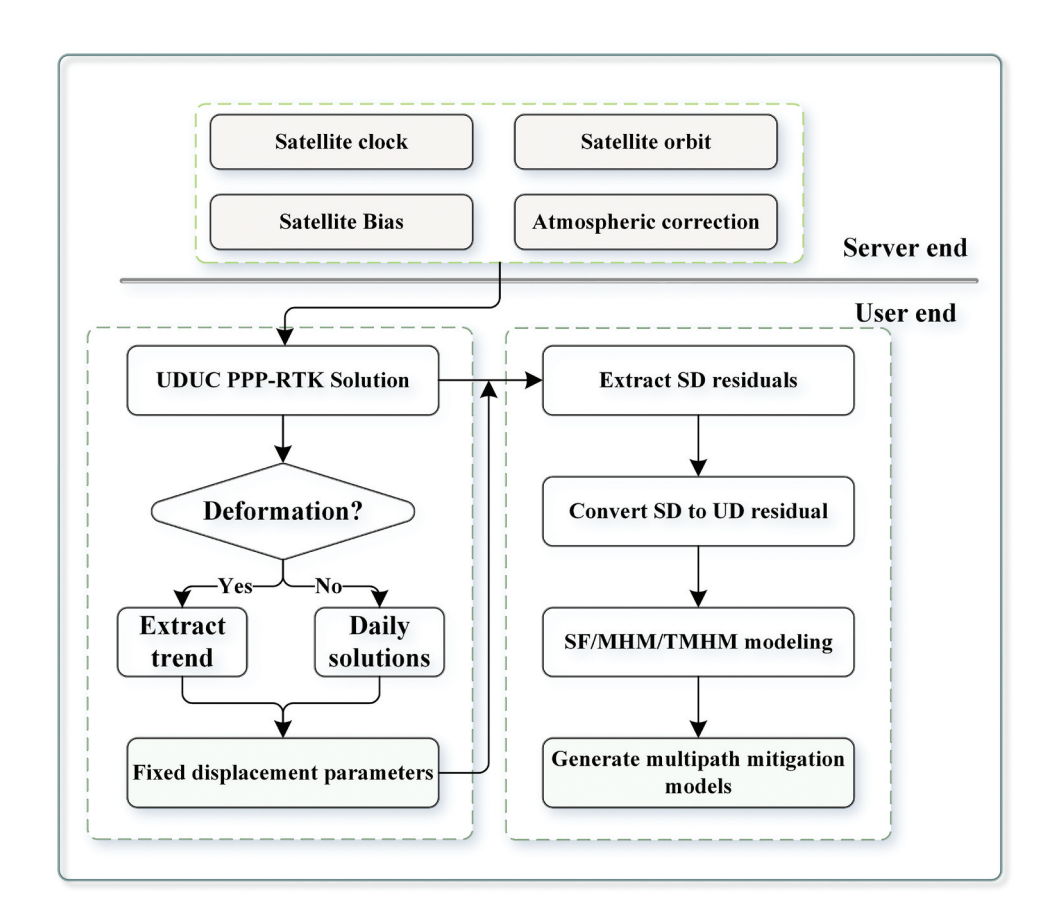


Figure 1. Multipath mitigation flowchart of UDUC PPP-RTK. Utilizing the SDtoUD multipath extraction method for both dynamic and static stations.

- - (II) In the absence of deformation, the daily solutions are adopted as the position parameters. In contrast, in the presence of deformation, the trend components are extracted from the original coordinate time series using the Complementary Ensemble Empirical Mode Decomposition (CEEMD) algorithm. Then, the position parameters are fixed to these trend values at each epoch. Notably, the proposed method is not sensitive to the choice of trend extraction technique, as long as the extracted time series effectively reflects the station's actual deformation.
 - (III) By accurately determining the position parameters for each epoch, observational residuals can be calculated using Equations (15) and (16).
 - (IV) Based on the extracted observational residuals, we establish an SF or MHM/TMHM multipath correction model and used for realtime multipath correction.

3. Data description

We use the dataset collected from the Heifangtai loess landslide group in Gansu Province, China, for validation. As shown in Figure 2, two GNSS monitoring stations (HF02, HF09) were deployed. Data from Day of Year (DOY) 007 to DOY 027 in 2021 was collected for the experiment. During the experiment period, HF02 (Figure 2(e)) station remained stable, while HF09 (Figure 2(d)) experienced continuous movement and finally collapsed at 13:01 UTC on DOY 027, as illustrated in Figure 2(b,c).

CORS stations in Gansu Province, China, were used as reference stations to calculate atmospheric correction products, depicted in Figure 2(a). All reference stations were equipped with Trimble NetR9 receivers and TRM 59,900.00 antennas, while the monitoring stations used Unicorecom UB4B0M lowcost boards and HighGain HG-GOYH7151 Geodetic Antennas. Two computational schemes are employed in this work that use different reference stations, as depicted in Figure 2(a). The average distance between two adjacent reference stations under Scheme 1 (yellow lines in Figure 2(a)) and Scheme 2 (green lines in Figure 2(a)) was 105 km and 214 km, respectively. Due to the partial data absence from some CORS stations, atmospheric correction products were calculated using data from DOY 007-019 in Scheme 1 and from DOY 020-027 in Scheme 2. The details of parameter settings in data processing are shown in Table 2.

4. Results and discussions

In this section, we assess the feasibility of the proposed SDtoUD and dynamic multipath extraction methods using the HF02 static station and HF09 dynamic station, respectively.

4.1. Results of different residual extraction methods

We first extracted the observational residuals based on the proposed method (SDtoUD) and conventional method (UD) with the data from a stable station (HF02) on DOY 013. Figure 3 illustrates the dualfrequency observation residuals and Power Spectral Density (PSD) of the G21 satellite at the HF02 station,

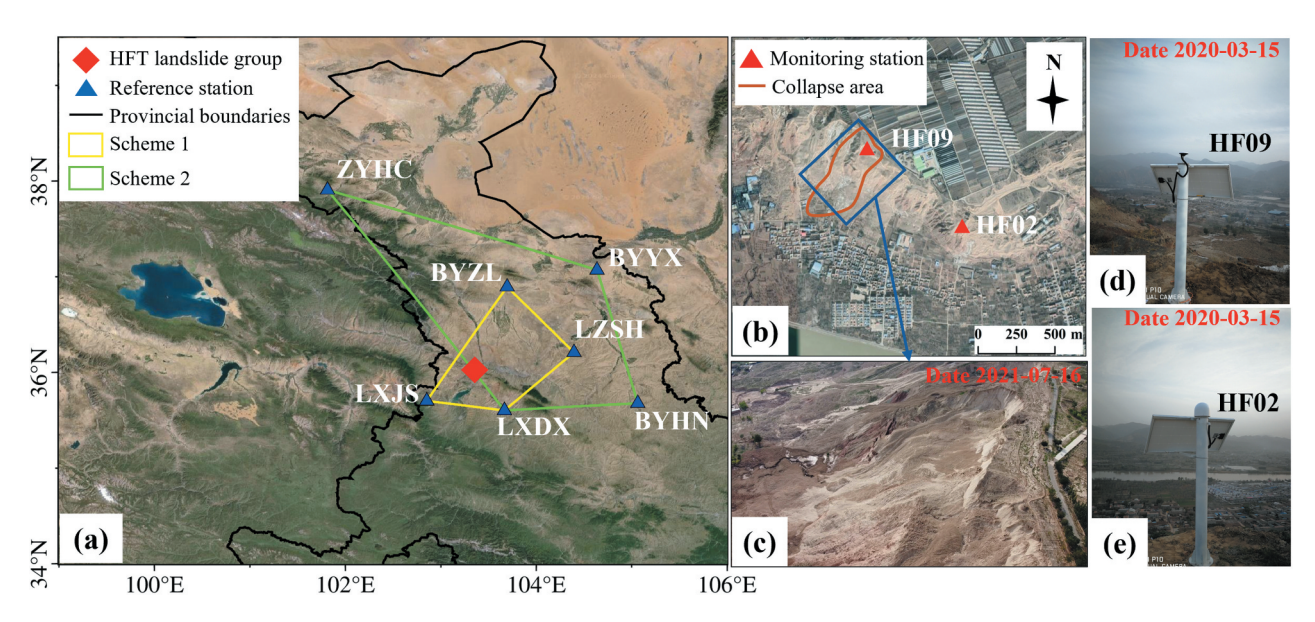


Figure 2. Overview of the study area reference stations and monitoring stations. (a) The location of the landslide area and the distribution of reference stations with two different spacings. (b) The location of the monitoring stations (image from Google Earth). (c) The collapse area where HF09 is located. (d) and (e) on-site photos of HF09 and HF02 stations, respectively.

Table 2. Data processing strategy used in this study.

| | 3 3, , |
|------------------------|--|
| ltem | Strategy |
| Observation | GPS L1&L2 |
| Sampling interval | 30 s |
| Parameter estimator | Kalman filter |
| Orbit and clock | Real-time products from the CNES |
| Code and phase biases | Corrected with the OSB products from the CNES |
| Cutoff angle | 7° |
| Priori precision | Code observations: 0.3 m; Phase observations: 0.3 cm |
| Tropospheric delays | Server-side: Zenith tropospheric Wet Delays (ZWD) estimated with random walk process, GPT2w for the mapping function. |
| | User: The additional augmentation information is used to provide the a priori ZWD value and the corresponding constraints. |
| lonospheric delays | Server-side: Estimated with random walk process to extract the values; |
| , | User: The additional augmentation information is used to provide the a priori ionospheric delay and the corresponding constraints. |
| AR strategy | WL uses rounding and NL uses LAMBDA; Partial ambiguity resolution. |

using two residual extraction methods. From the left column of Figure 3, it can be observed that the residuals extracted by the SDtoUD method exhibit a similar pattern to those from the UD method, but with a lower noise level. The PSD of the SDtoUD and UD residuals highlights this difference. High-frequency noise is prone to mix with high-frequency multipath, so a lower noise level in the high-frequency band indicates better performance in extracting high-frequency multipath (Dong et al. 2016; Geng, Jiang, and Liu 2017). The PSD results further confirm that the proposed method performs better in accurately

extracting residuals, particularly in the high-frequency range (greater than 200 s). This improvement is mainly attributed to the SDtoUD method's advantage in eliminating the influence of receiver clock offset, which is considered white noise and typically exhibits high-frequency characteristics (Ge et al. 2019).

As mentioned in Section 2.3, the extracted residuals may be affected when other satellites' NL SD ambiguities encounter incorrect fixes. To evaluate the robustness of the proposed method, a two-cycle error was added to the NL SD ambiguity of the G21 satellite to simulate the ambiguity-fixing errors. Figure 4 shows the ambiguities and residuals of the G06 satellite before and after adding ambiguity errors on the G21 satellite, extracted using both methods. During the fixed solutions period, it can be observed that, the SDtoUD derived ambiguities for the G06 satellite remain resilient to the NL SD ambiguity errors originating from the G21 satellite. Consequently, the residuals pertaining to the G06 satellite are minimally impacted, compared to those derived from UD method. This phenomenon can be attributed to the independent estimation of SD ambiguities for each satellite during the SDtoUD residual extraction process (Equations (8) and (9)). As a result, only the ionospheric and tropospheric parameters are affected during the constraint updating process (Equations (10) and (11)). In contrast, for UD residual, both the UD ambiguity and receiver clock offset parameters are influenced by such incorrect fixes.

Additionally, during the conversion process from SD to UD residual (Equation (16)), while the

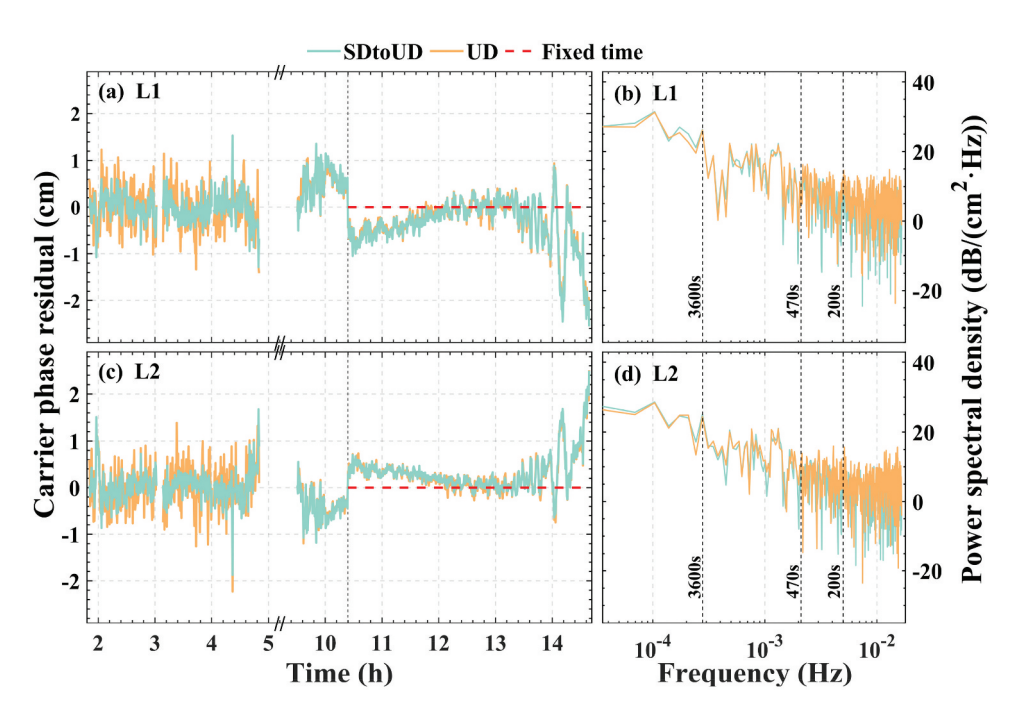


Figure 3. Residuals and corresponding PSD for G21 satellite at the HF02 station on DOY 013. L1 frequency in (a) and (b), and L2 frequency in (c) and (d). The red dashed lines indicate the period of ambiguity-fixed.

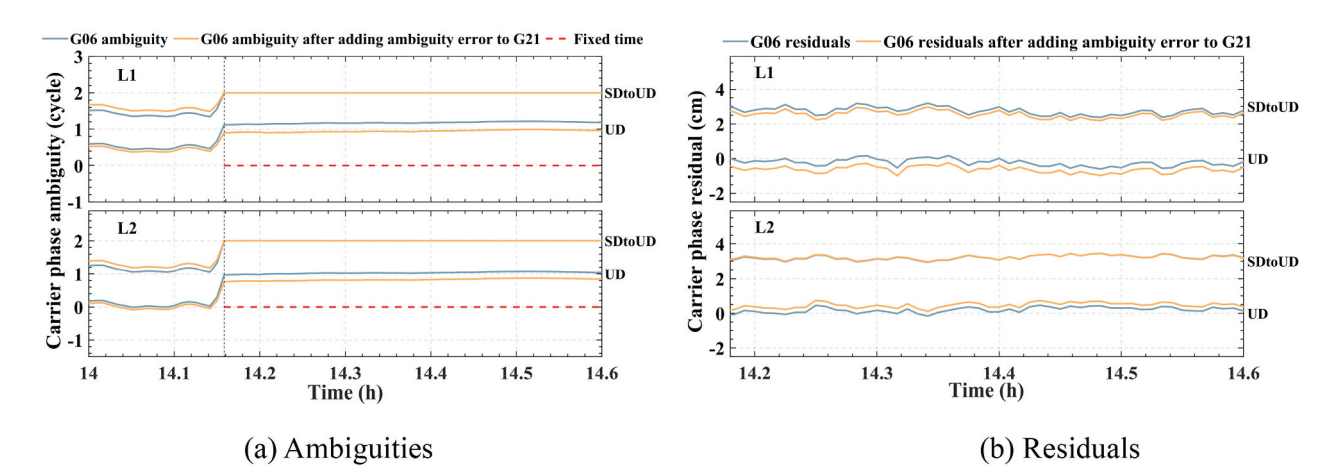


Figure 4. Dual-frequency ambiguities (a) and residuals (b) for G06 satellite before (blue lines) and after (yellow lines) adding NL SDs ambiguity errors to the G21 satellite, extracted both computation methods with the HF02 data on DOY 013. (b) Shows only the fixed solution. Each sequence has a vertical offset of several cycles or 3 cm for clarity.

introduction of a zero-mean constraint in the coefficient matrix may lead to some error propagation, it can be observed from the right column of Figure 4 that the residuals of the G21 satellite have minimal impact on the SDtoUD residuals of G06. This is because, during the conversion process, the SD residuals of the G21 satellite are primarily constrained within its own SDtoUD residuals, resulting in very little error being transferred to other satellites. Compared to the impact of incorrect ambiguity parameters from G21 on the residual extraction for G06, the error introduced into G06's SDtoUD residuals through the SDto-UD conversion process is significantly smaller. Moreover, only the multipath values from fixed solutions will be adopted for correction purposes.

We further extracted pseudorange residuals from the HF02 station for DOY 007-013, and carrier-phase residuals using the SDtoUD and UD methods. Based on these data, we constructed multipath correction models using SF, MHM, and TMHM methods, respectively. The SF model used Wavelet Transform (WT) filtering and multipath correction models built from residuals over 1-7 days. The MHM/TMHM models are both investigated using 5 days of residuals and a grid with a spatial resolution of $1^{\circ}\times1^{\circ}$. Figure 5 shows the positioning errors before and after multipath model correction on DOY 014 and the details of some time periods. Compared to unfiltered results, both SDtoUD and UD correction results can significantly improve the positioning performance, with SDtoUD showing more noticeable improvements at certain epochs (e.g. around 21 h).

Figure 6 presents the average Root Mean Squared Error (RMSE) of positioning errors after multipath mitigation. It can be observed that the SDtoUD method shows better improvement than the UD method, primarily due to the stronger robustness and the advantage of eliminating receiver clock offset parameter errors inherent in the SDtoUD method. However, when constructing the multipath correction

model using only 1 or 2 days of residuals, the positioning results in the Up direction deteriorated. This is likely due to inaccuracies in atmospheric parameter estimation, causing the multipath correction model to be affected by atmospheric errors. Such impacts can be mitigated by using multi-day averaging residuals, i.e. more than 3 days (Geng et al. 2018).

4.2. Results of dynamic multipath extraction method

We further validate the proposed method using data from a monitoring station in a rapid deformation phase, i.e. HF09 in Figure 2. The key to accurately extracting multipath errors lies in obtaining precise position parameters. As shown in Figure 7, the displacement time series from DOY 022–026 is first calculated using the PPP-RTK technique. Then, the trend of displacement sequence is extracted using the CEEMD algorithm. It can be found that the trend series effectively eliminates high-frequency noise and low-frequency errors, accurately reflecting the actual deformation. This trend is then used as the dynamic position parameter to extract observational residuals with the proposed method in dynamic scenarios.

Using DOY 025 as an example, the displacement in the north and up directions reached 1.7 cm and 3.9 cm, respectively. Figure 8 displays two panels illustrating the residuals of four satellites obtained using the proposed dynamic method and the conventional static method (i.e. without accounting for station deformation), respectively. The bottom row in Figure 8 shows the coordinate differences between these two methods. It can be seen that the residuals extracted by both the static and dynamic methods exhibit similar patterns over a one-day period, and this is also true for the results of the 1-day (1 d) residuals and the averaged residuals over 3 consecutive days (3 d). These findings

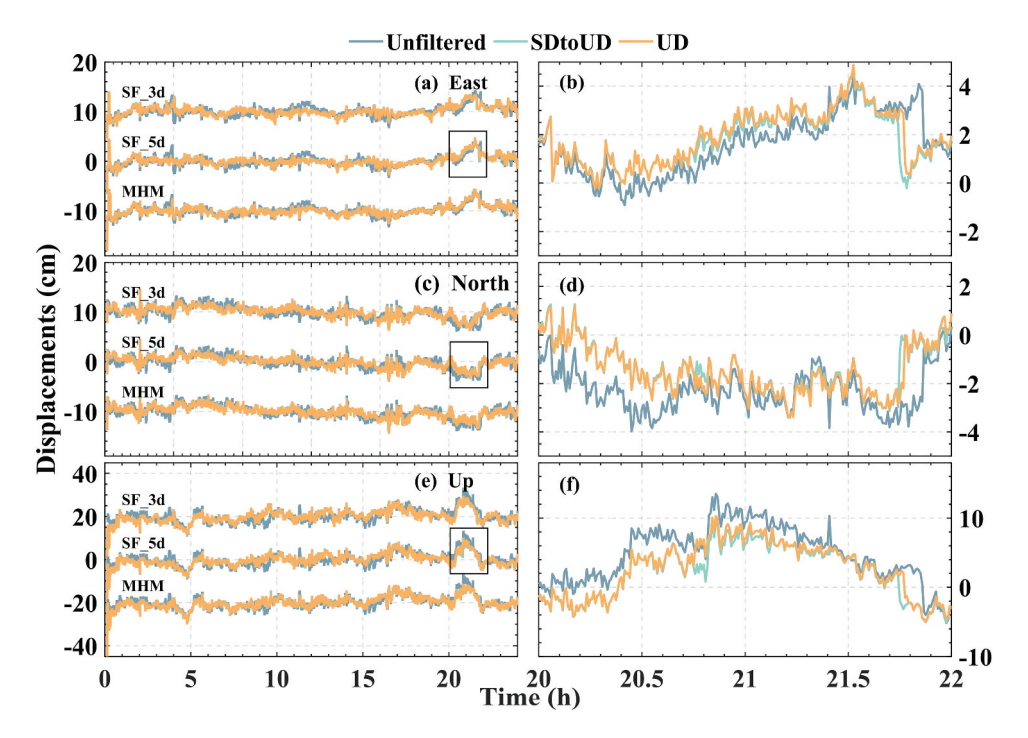


Figure 5. Positioning errors for HF02 station on DOY 014 before (unfiltered) and after multipath correction using different extraction methods. (a), (c), and (e) display the full time series; the black-boxed segments are enlarged in (b), (d), and (f). "SF_3d" and "SF_5d" denote SF using 3 days and 5 days of residuals, respectively. Horizontal and vertical time series have vertical offsets of 10 cm and 20 cm, respectively.

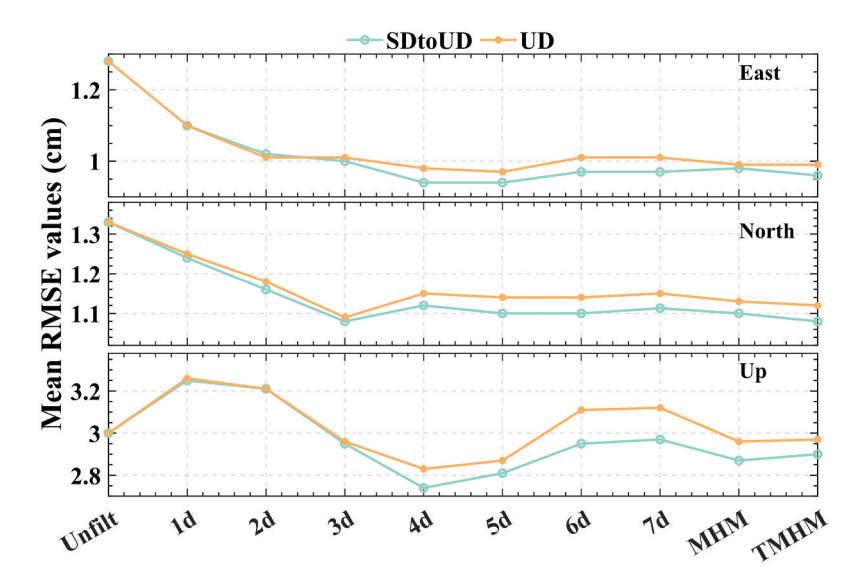


Figure 6. Average RMSE of HF02 station positioning errors after correction using MHM/TMHM and SF models (with residuals from the previous 1d–7d). The SF correction results using different days of residuals are labeled as 1d–7d.

indicate that even with centimeter-level deformation, the repeatability of multipath errors remains largely unaffected. However, there are significant systematic errors between the residuals extracted by the two methods, and these differences increase with the coordinate differences and the number of observation days. These systematic errors result from the assumption of the conventional approach that the monitoring points are stable, whereas the proposed dynamic method effectively eliminates such errors.

Figure 9 shows the unfiltered displacement time series and those corrected using two multipath extraction methods for HF09 over a continuous 48-h period from DOY 025-026. In the east direction, the results of both methods are relatively consistent compared to the unfiltered results. However, in the north and up directions, the results corrected using the static method exhibit some offset. This is primarily because the larger deformations in these directions cause the static

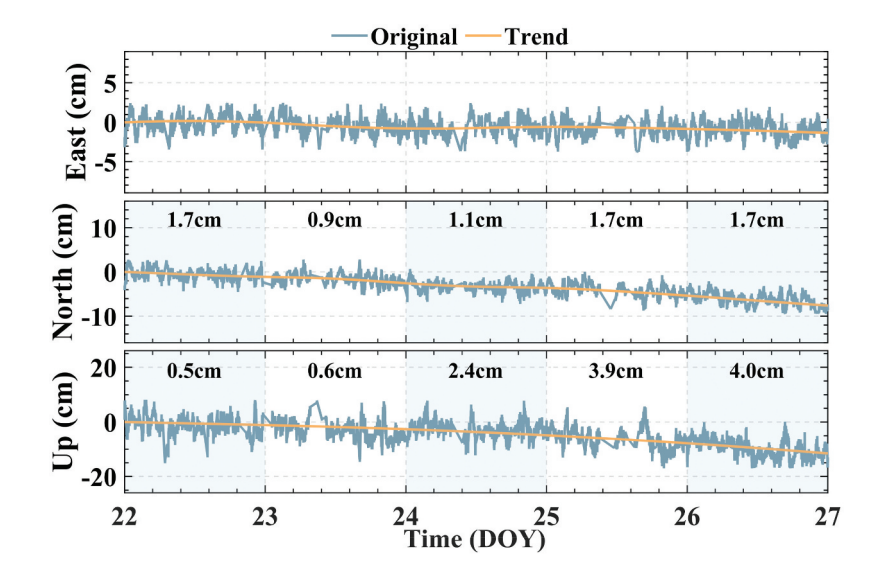


Figure 7. Preprocessed PPP-RTK coordinate time series and trends extracted using the CEEMD method. In which the trend at the first epoch is regarded as the initial position. The numbers in the north and up components represent the daily displacement (the trend at the last epoch of each day minus the trend at the first epoch).

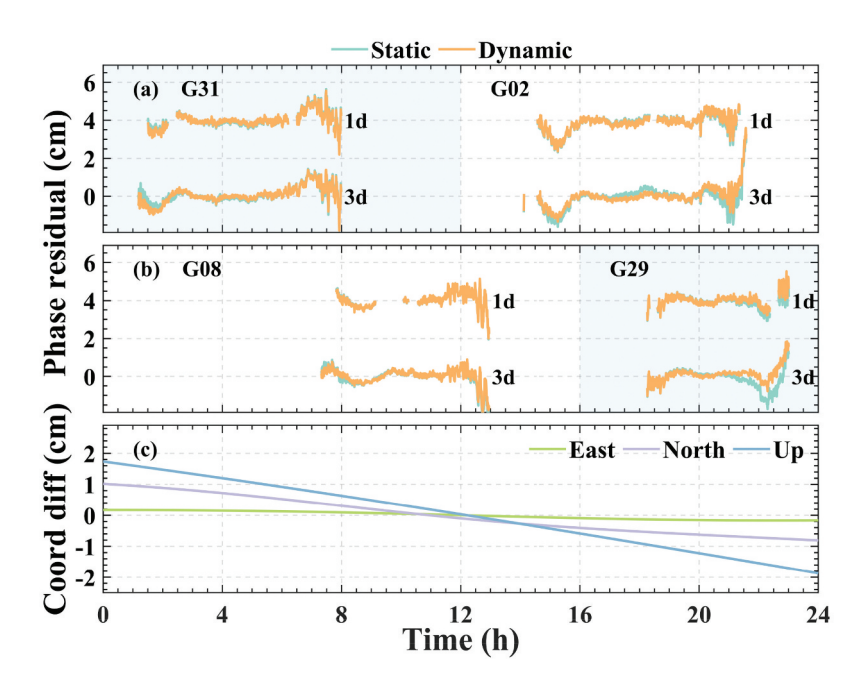


Figure 8. Residuals of each satellite extracted using the dynamic and the traditional static method (a and b), and the difference in position parameters between the two methods (c). "3d" indicates the results obtained by averaging residuals over 3 consecutive days.

method to mistakenly incorporate displacement information from the modeling day into the correction day. In contrast, the time series corrected using the proposed dynamic method aligns more closely with the original displacement trend and shows more significant multipath correction effects.

Figure 10 shows the average RMSE of positioning errors after correction using the MHM, TMHM, and SF (with residuals from the previous 1 d–7 d) models.

The results indicate that the proposed dynamic method improves correction effectiveness regardless of the model used. Additionally, while the conventional static method shows some effectiveness when using only 1d residuals for modeling, as the number of days used for multipath modeling increases, errors caused by position parameters begin to accumulate in the traditional static method, making it unsuitable for multipath correction in dynamic deformation data.

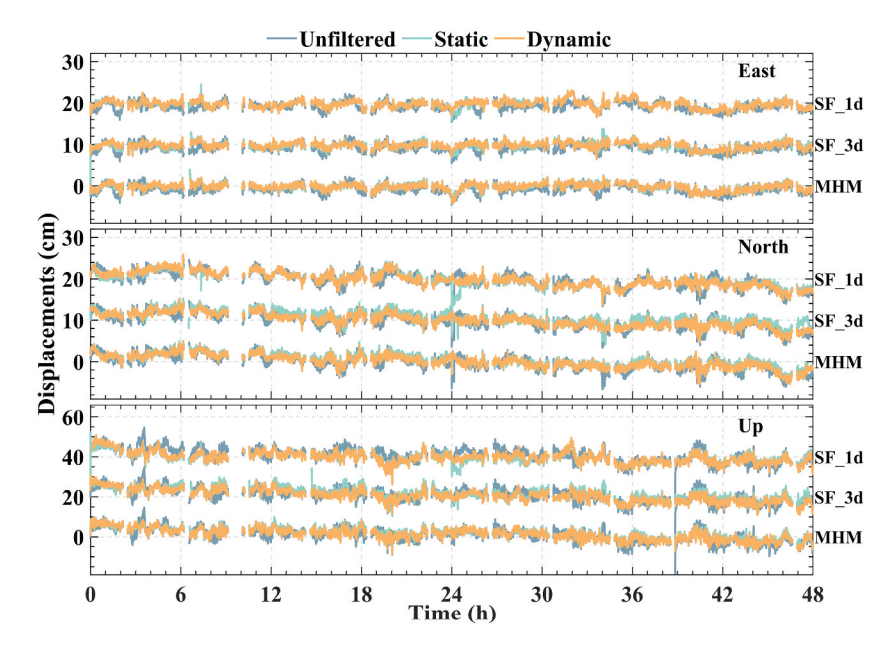


Figure 9. Unfiltered results and displacement time series corrected using dynamic and static multipath extraction methods. "SF_1d" and "SF_3d" represent the results of SF modeling corrections using residuals from the previous 1 day and 3 days, respectively. Horizontal and vertical time series have vertical offsets of 10 cm and 20 cm, respectively.

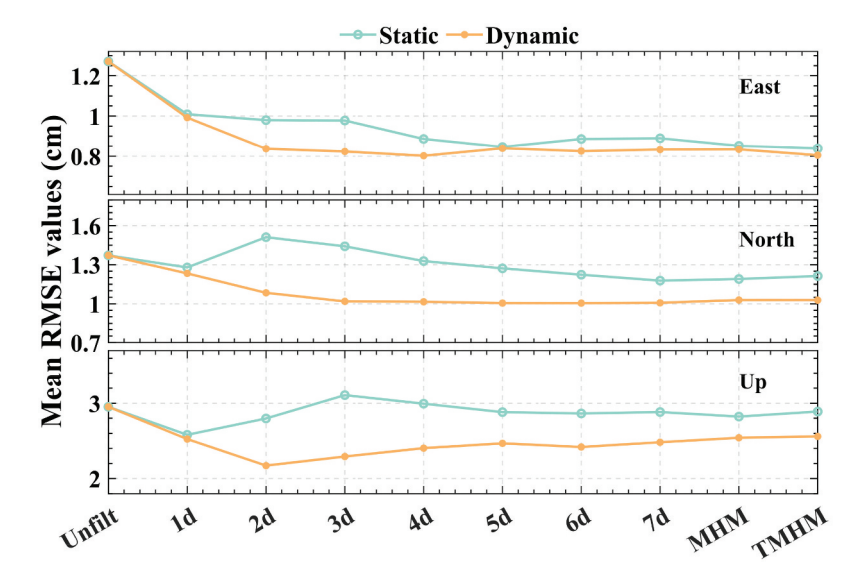


Figure 10. Average RMSE of HF09 station positioning errors after correction using MHM/TMHM and SF models (with residuals from the previous 1d-7d). The SF correction results using different days of residuals are labeled as 1d–7d.

4.3. Positioning performance of PPP-RTK in dynamic landslide monitoring

To validate the effectiveness of real-time PPP-RTK and the proposed multipath mitigation algorithm in landslide deformation monitoring, this study processed data from the HF09 station covering the entire period of the landslide's instability and collapse from DOY 010–027. Figure 11 presents the unfiltered PPP-RTK results and the displacement time series corrected using the SF model with both static and dynamic multipath extraction methods. To achieve optimal multipath mitigation, the static and dynamic methods used 1-day and 3-day

residuals for modeling, respectively (based on Figure 10). The results indicate that all three solutions effectively capture the deformation trend of the landslide. However, the unfiltered and static method displacement time series contain more outliers, while those are rarely present in the results corrected using the proposed dynamic method.

To investigate the impact of reference station network density on PPP-RTK positioning performance, we further calculated the HF09 displacements during DOY 010–019 with atmospheric products from computational Scheme 2. Table 3 summarizes the fixed rates and RMSE of the original unfiltered displacement results, and those

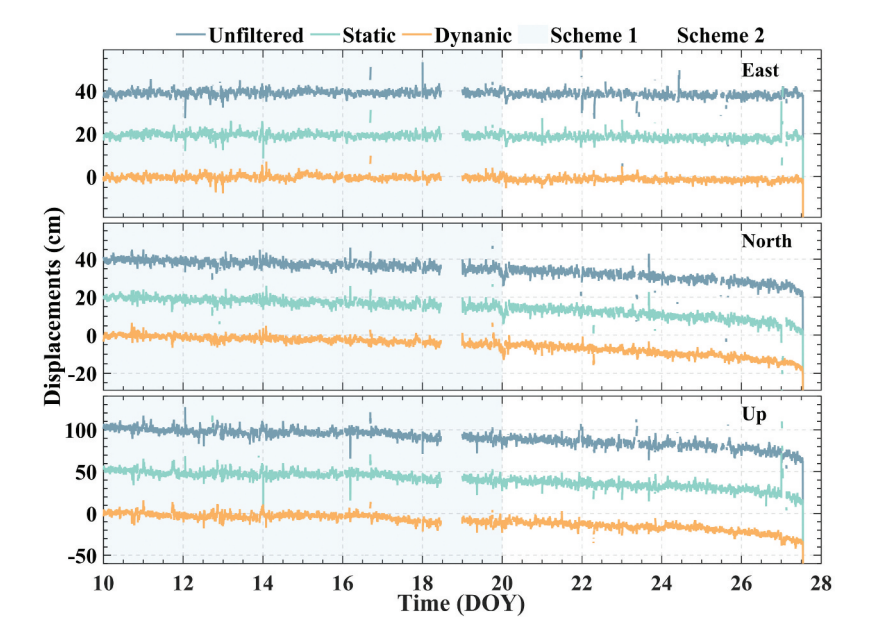


Figure 11. Unfiltered and SF mitigated displacement monitoring time series for HF09 station (showing only ambiguity-fixed solutions). The atmospheric products of DOY 010–019 and 020–027 were calculated using Scheme 1 and Scheme 2, respectively. The horizontal and vertical results have vertical offsets of 20 cm and 50 cm for clarity, respectively.

Table 3. Accuracy statistics of unfiltered and multipath mitigated results for HF09 station.

| Туре | DOY | Scheme | Unfiltered | | | Static | | | Dynamic | | |
|------------------------|---------|------------|------------|-------|-----|--------|-------|-----|---------|-------|-----|
| Fixed-rate (%) | 010-019 | S 1 | | 97.67 | | | 97.80 | | | 98.13 | |
| | | S2 | | 96.77 | | | 97.24 | | | 97.60 | |
| | 020-027 | S2 | | 91.24 | | | 95.67 | | | 98.01 | |
| Correct fixed-rate (%) | 010-019 | S 1 | 98.27 | | | 98.35 | | | 98.49 | | |
| | | S2 | | 98.13 | | | 97.97 | | | 98.49 | |
| | 020-027 | S2 | | 97.22 | | | 97.71 | | | 98.75 | |
| Direction | | | Ε | N | U | Ε | N | U | Ε | N | U |
| RMSE (cm) | 010-019 | S 1 | 1.4 | 1.5 | 3.8 | 1.3 | 1.4 | 4.0 | 1.1 | 1.2 | 3.2 |
| | | S2 | 1.6 | 1.6 | 3.9 | 1.4 | 1.4 | 3.8 | 1.1 | 1.2 | 3.3 |
| | 020-027 | S2 | 1.8 | 2.2 | 4.8 | 1.7 | 2.2 | 4.7 | 0.9 | 1.3 | 3.2 |

from the static and proposed dynamic multipath extraction methods under different reference station networks. Scheme 1 shows noteworthy improvements in fixed rate and correct fixed rate compared to Scheme 2 in the original unfiltered results, indicating the significant impact of the reference network density on the PPP-RTK performance for end users. Although the conventional static method shows slight enhancements after correction, the proposed dynamic method shows substantial advancements in fixed rate and reduced RMSE when compared to the unfiltered and static methods. The RMSE of ambiguity-fixed solutions using the dynamic method are 1.1 cm, 1.2 cm, and 3.2 cm in the east, north, and up directions for Scheme 1 over DOY 010-019, and 1.0 cm, 1.3 cm, and 3.3 cm for Scheme 2 over DOY 010-027, corresponding to improvements of 15%, 14%, 20% for Scheme 1 and 37%, 28%, and 23% for Scheme 2 relative to the traditional static method.

5. Conclusions

Accurate extraction of observational residuals is crucial to the multipath mitigation techniques in PPP-RTK.

This paper proposes a new multipath extraction method that converts SD residuals to UD residuals to better extraction multipath in a PPP-RTK model. Experimental validation with data from a landslide site using SF, MHM, and TMHM models shows that the proposed method effectively eliminates receiver clock offset and reduces the influence of other satellite ambiguity parameters, allowing accurate and robust residuals to be observed. The multipath mitigation models built using these residuals also significantly improve positioning performance.

Additionally, for dynamic deformation monitoring applications, this paper proposes a multipath extraction method based on dynamic position parameters. Analysis of real landslide dynamic monitoring data demonstrates that the proposed method surpasses traditional static methods in ambiguity-fixed rate and positioning accuracy. Under wide-area reference station networks with average spacings of 105 km and 214 km, the realtime PPP-RTK landslide monitoring accuracy after correction using the proposed method can reach 1.1 cm, 1.2 cm, 3.2 cm, and 1.0 cm, 1.3 cm, 3.3 cm in the east, north, up directions, respectively. This represents improvements of 15%, 14%, 20%, and 37%, 28%, 23% in accuracy compared to traditional methods. However, it is worth noting that in more complex monitoring scenarios or when the deformation rate further increases, the spatiotemporal repeatability of multipaths may be compromised. The applicability of the SF and MHM models in such highly dynamic environments requires further validation in the future research.

Disclosure statement

No potential conflict of interest was reported by the author(s).

Funding

This work is funded by the National Natural Science Foundation of China [Grant number 42127802], the National Key Research and Development Program of China [Grant number 2024YFC3012603], the Natural Science Basic Research Program of Shanxi Province [Grant number 2025JC-YBMS-251], the Innovation Team of ShaanXi Provincial Tri-Qin Scholars with Geoscience Big Data and Geohazard Prevention (2022), and the Fundamental Research Funds for the Central Universities, CHD [Grant number 300102263202].

Notes on contributors

Xinrui Li is currently pursuing a Ph.D. at Chang'an University in Xi'an, China. His current research focuses on GNSS unmodeled error mitigation.

Bao Shu is an associate professor at Chang'an University, Xi'an, China. His research activities mainly include GNSS high-precision positioning algorithms and applications.

Xuanyu Qu obtained his Ph.D. in the Department of Land Surveying and Geo-Informatics, the Hong Kong Polytechnic University, China. His current research focuses on GNSS high-precision positioning and multi-sensor integration for structural health monitoring.

Qin Zhang is a professor at Chang'an University, Xi'an, China. Her current research activities have been mainly related to GNSS and InSAR theory and applications.

Yunging Tian is currently pursuing a doctoral degree at Chang'an University, Xi'an, China. His current research mainly focuses on GNSS precise positioning services and their integrity monitoring.

Guanwen Huang is a professor of Chang'an University, Xi'an, China. His research activities include precise point positioning theory, real-time satellite clock model, and their application.

Li Wang is a professor of Chang'an University, Xi'an, China. His current research interest is in engineering surveying, spatial positioning technology, deformation monitoring, and prediction.

ORCID

Xuanyu Qu http://orcid.org/0000-0001-8836-4420

Data availability statement

The real-time orbit, clock, and OSB products were downloaded from the Centre National d'Etudes Spatiales (http://www.ppp-wizard.net/products/REAL_ TIME/).

References

Atkins, C., and M. Ziebart. 2016. "Effectiveness of Observation-Domain Sidereal Filtering for GPS Precise Point Positioning." GPS Solutions 20 (1): 111-122. https://doi.org/10.1007/s10291-015-0473-1.

Azarbad, M. R., and M. R. Mosavi. 2014. "A New Method to Mitigate Multipath Error in Single-Frequency GPS Receiver with Wavelet Transform." GPS Solutions 18 (2): 189-198. https://doi.org/10.1007/s10291-013-0320-1.

Bock, Y. 1991. "Continuous Monitoring of Crustal Deformation." GPS World 2 (6): 40-47.

Chen, D., S. Ye, F. Xia, X. Cheng, H. Zhang, and W. Jiang. 2022. "A Multipath Mitigation Method in Long-Range RTK for Deformation Monitoring." GPS Solutions 26 (3): 96. https://doi.org/10.1007/s10291-022-01281-9.

Choi, K., A. Bilich, K. M. Larson, and P. Axelrad. 2004. "Modified Sidereal Filtering: Implications for High-Rate GPS Positioning." Geophysical Research Letters 31 (22). https://doi.org/10.1029/2004GL021621.

Cina, A., P. Dabove, A. M. Manzino, and M. Piras. 2015. "Network Real Time Kinematic (NRTK) Positioning-Description, Architectures and Performances." Satellite Positioning-Methods, Models and Applications: 23-45. https://doi.org/10/5772/59083.

Cohen, C. E., and B. W. Parkinson. February 2-6, 1991. "Mitigating Multipath Error in GPS Based Attitude Determination." In Proceedings of the Annual Rocky Mountain Guidance and Control Conference, Keystone,

Dai, W., X. Ding, and J. Zhu. 2008. "Study on Multipath Effect in Structural Health Monitoring Using GPS." Journal of Geodesy and Geodynamics 28 (1): 65-71.

Dai, W., D. Huang, and C. Cai. 2014. "Multipath Mitigation via Component Analysis Methods for GPS Dynamic Deformation Monitoring." GPS Solutions 18 (3): 417-428. https://doi.org/10.1007/s10291-013-0341-9.

Dong, D., M. Wang, W. Chen, Z. Zeng, L. Song, Q. Zhang, M. Cai, Y. Cheng, and J. Lv. 2016. "Mitigation of Multipath Effect in GNSS Short Baseline Positioning by the Multipath Hemispherical Map." Journal of Geodesy 90 (3): 255-262. https://doi.org/10.1007/s00190-015-

Elosegui, P., J. L. Davis, R. T. K. Jaldehag, J. M. Johansson, A. E. Niell, and I. I. Shapiro. 1995. "Geodesy Using the Global Positioning System; the Effects of Signal Scattering on Estimates of Site Position." Journal of Geophysical Research 100 (B6): 9921-9934. https://doi.org/10.1029/

Gao, R., Z. Liu, R. Odolinski, Q. Jing, J. Zhang, H. Zhang, and B. Zhang. 2023. "Hong Kong-Zhuhai-Macao Bridge Deformation Monitoring Using PPP-RTK with

- Multipath Correction Method." GPS Solutions 27 (4). https://doi.org/10.1007/s10291-023-01491-9.
- Ge, M., G. Gendt, M. Rothacher, C. Shi, and J. Liu. 2008. "Resolution of GPS Carrier-Phase Ambiguities in Precise Point Positioning (PPP) with Daily Observations." Journal of Geodesy 82 (7): 389-399. https://doi.org/10. 1007/s00190-007-0187-4.
- Ge, Y., F. Zhou, T. Liu, W. Qin, S. Wang, and X. Yang. 2019. "Enhancing Real-Time Precise Point Positioning Time and Frequency Transfer with Receiver Clock Modeling." *GPS Solutions* 23 (1). https://doi.org/10.1007/s10291-018-0814-y.
- Geng, J., P. Jiang, and J. Liu. 2017. "Integrating GPS with GLONASS for High-Rate Seismogeodesy: High-Rate Multi-GNSS." Geophysical Research Letters 44 (7): 3139-3146. https://doi.org/10.1002/2017GL072808.
- Geng, J., Y. Pan, X. Li, J. Guo, J. Liu, X. Chen, and Y. Zhang. 2018. "Noise Characteristics of High-Rate Multi-GNSS for Subdaily Crustal Deformation Monitoring." Journal of Geophysical Research Solid Earth 123 (2): 1987-2002. https://doi.org/10.1002/2018JB015527.
- Guo, Z., Y. Yao, C. Xu, et al. 2024. "Method for Establishing the Multipath Adaptive Mitigation Model Considering Deformation Displacement of Monitoring Stations." Geo-Spatial Information Science: 1-16. https://doi.org/10. 1080/10095020.2024.2436859.
- Kaloop, M. R., C. O. Yigit, A. El-Mowafy, et al. 2020. "Hybrid Wavelet and Principal Component Analyses Approach for Extracting Dynamic Motion Characteristics from Displacement Series Derived from Multipath-Affected High-Rate GNSS Observations." Remote Sensing 12 (1): 79. https://doi.org/10.3390/ rs12010079.
- Kazmierski, K., R. Zajdel, and K. Sośnica. 2020. "Evolution of Orbit and Clock Quality for Real-Time Multi-GNSS Solutions." GPS Solutions 24 (4): 111. https://doi.org/10. 1007/s10291-020-01026-6.
- Li, X., G. Dick, M. Ge, S. Heise, J. Wickert, and M. Bender. 2014. "Real-Time GPS Sensing of Atmospheric Water Vapor: Precise Point Positioning with Orbit, Clock, and Phase Delay Corrections." Geophysical Research Letters 3615-3621. https://doi.org/10.1002/ 2013GL058721.
- Li, X., L. Wang, X. Qu, S. Zhang, B. Shu, and H. Xu. 2024. GPS Multipath Mitigation Method Coordinate-Domain Considering the Effects of Gross Errors and Missing Data." Measurement 225:114035. https://doi.org/10.1016/j.measurement.2023.114035.
- Li, X., X. Zhang, and M. Ge. 2011. "Regional Reference Network Augmented Precise Point Positioning for Instantaneous Ambiguity Resolution." Journal of Geodesy 85 (3): 151-158. https://doi.org/10.1007/ s00190-010-0424-0.
- Liu, G., X. Zhang, and P. Li. 2019. "Estimating Multi-Frequency Satellite Phase Biases of BeiDou Using Maximal Decorrelated Linear Ambiguity Combinations." GPS Solutions 23 (2): 42. https://doi.org/10.1007/s10291-019-0836-0.
- Liu, T., W. Jiang, D. Laurichesse, H. Chen, X. Liu, and J. Wang. 2020. "Assessing GPS/Galileo Real-Time Precise Point Positioning with Ambiguity Resolution Based on Phase Biases from CNES." Advances in Space Research 66 (4): 810-825. https://doi.org/10.1016/j.asr. 2020.04.054.
- Lovse, J. W., W. F. Teskey, G. Lachapelle, and M. E. Cannon. 1995. "Dynamic Deformation Monitoring of Tall Structure Using GPS Technology." Journal of Surveying

- Engineering 121 (1): 35-40. https://doi.org/10.1061/ (ASCE)0733-9453(1995)121:1(35).
- Lu, R., W. Chen, D. Dong, Z. Wang, C. Zhang, Y. Peng, and C. Yu. 2021. "Multipath Mitigation in GNSS Precise Point Positioning Based on Trend-Surface Analysis and Multipath Hemispherical Map." GPS Solutions 25 (3): 119. https://doi.org/10.1007/s10291-021-01156-5.
- Odijk, D., B. Zhang, A. Khodabandeh, R. Odolinski, and P. J. G. Teunissen. 2016. "On the Estimability of Parameters in Undifferenced, Uncombined GNSS Network and PPP-RTK User Models by Means of S-System Theory." Journal of Geodesy 90 (1): 15-44. https://doi.org/10.1007/s00190-015-0854-9.
- Ogutcu, S., S. Alcay, H. Duman, B. N. Ozdemir, and C. Konukseven. 2023. "Static and Kinematic PPP-AR Performance of Low-Cost GNSS Receiver in Monitoring Displacements." Advances in Space Research 72 (11): 4795–4808. https://doi.org/10.1016/j.asr.2023.09.025.
- Qu, X., X. Ding, Y. Xu, and W. Yu. 2023. "Real-Time Outlier Detection in Integrated GNSS and Accelerometer Structural Health Monitoring Systems Based on a Robust Multi-Rate Kalman Filter." Journal of Geodesy 97 (4): 38. https://doi.org/10.1007/s00190-023-01724-2.
- Ragheb, A. E., P. J. Clarke, and S. J. Edwards. 2007. "GPS Sidereal Filtering: Coordinate- and Carrier-Phase-Level Strategies." Journal of Geodesy 81 (5): 325-335. https:// doi.org/10.1007/s00190-006-0113-1.
- Shu, B., Y. Tian, X. Qu, P. Li, L. Wang, G. Huang, Y. Du, and Q. Zhang. 2024. "Estimation of BDS-2/3 Phase Observable-Specific Signal Bias Double-Differenced Model: An Exploration of Fast BDS-2/3 Real-Time PPP." GPS Solutions 28 (2): 88. https://doi.org/10.1007/s10291-024-01632-8.
- Teunissen, P., D. Odijk, and B. Zhang. 2010. "PPP-RTK: Results of CORS Network-Based PPP with Integer Ambiguity Resolution." Journal of Aeronautics, Astronautics and Aviation, Series A 42 (4): 223-230.
- Wang, H., Z. Zhang, Y. Dong, W. Zhan, and Y. Li. 2023. "Real-Time Multipath Mitigation Based Spatiotemporal Correlations in BDS Precise Point Positioning." GPS Solutions 28 (1): 37. https://doi.org/ 10.1007/s10291-023-01576-5.
- Wang, Z., W. Chen, D. Dong, M. Wang, M. Cai, C. Yu, Z. Zheng, and M. Liu. 2019. "Multipath Mitigation Based on Trend Surface Analysis Applied to Dual-Antenna Receiver with Common Clock." GPS Solutions 23 (4): 1-15. https://doi.org/10.1007/s10291-019-0897-0.
- Wübbena, G., M. Schmitz, and A. Bagge. 2005. "PPP-RTK: Precise Point Positioning Using State-Space Representation in RTK Networks." The 18th International Technical Meeting of the Satellite Division of the Institute of Navigation (ION GNSS 2005), Long Beach, California, USA., September 13-16.
- Zhang, B., Y. Chen, and Y. Yuan. 2019. "PPP-RTK Based on Undifferenced and Uncombined Observations: Theoretical and Practical Aspects." Journal of Geodesy 93 (7): 1011-1024. https://doi.org/10.1007/s00190-018-1220-5.
- Zheng, K., X. Zhang, P. Li, X. Li, M. Ge, F. Guo, J. Sang, and H. Schuh. 2019. "Multipath Extraction and Mitigation for High-Rate Multi-GNSS Precise Point Positioning." Journal of Geodesy 93 (10): 2037-2051. https://doi.org/ 10.1007/s00190-019-01300-7.
- Zhong, P., X. Ding, L. Yuan, Y. Xu, K. Kwok, and Y. Chen. 2010. "Sidereal Filtering Based on Single Differences for Mitigating GPS Multipath Effects on Short Baselines." Journal of Geodesy 84 (2): 145-158. https://doi.org/10. 1007/s00190-009-0352-z.